Hypothesis of a Violation of Lorentz Invariance in the Aether Theory and Confirmation by the Experiments of D. C. Miller

Sebastian Pliet*

17th September 2021 / 1.1

It is hypothesized that the refractive index of moving gases in their rest frame becomes anisotropic. Therefore interferometers with air in the light path should be able to measure a phase shift. The theoretical signal is derived from Lorentz's aether theory. The hypothesis is tested against historical data from Dayton C. Miller's experiments on Mount Wilson in 1925–1926. A suitable signal is found in selected data, confirming the aether theory. Using curve fitting, the speed v and the apex, in equatorial coordinates (α, δ), of the motion of the solar system in the aether were determined. The smallest deviation of the theory from the data results with the parameters

$$v = (326 \pm 17)\ \text{km/s}, \quad \alpha = (11.0 \pm 0.2)\ \text{h}, \quad \delta = (\text{-}11 \pm 5)^\circ.$$

*aetherise@gmx.de

Contents

1. Motivation

One of the big questions in physics is the question of the true meaning of the Lorentz transformation [2]. There are at least two possibilities. In the aether theory of Lorentz [3], it describes a symmetry of electromagnetism, which propagates in a certain reference frame, the aether. In the Special Theory of Relativity (STR) of Einstein [4] it is interpreted as relative simultaneity or spacetime [5], a fundamental nature of space and time without a preferred frame of reference.

Although there is a preferred frame of reference in the aether theory, it was postulated that it could not be discovered. Thus both theories provide the same description of electrical and optical phenomena in moving bodies.

However, the fundamentally different nature of the two theories gives rise to the assumption that a distinction is possible.[1]

2. Hypothesis

The first experiments to discover the aether tried to measure a change in the time of flight of light rays by means of interferometers. In any case, the Earth on which the experiment takes place moves around the sun and thus through the aether, which should lead to a measurable phase shift [6]. These first experiments did not deliver the expected result, which also led to the further development of the aether theory [7].

The hypothesis now concerns exactly this kind of experiments, i.e. large interferometers whose light rays pass through air.

2.1. Light path in vacuum and in solids

It follows from the aether theory that the mean speed of light is constant on closed paths. If a Michelson interferometer is operated in a vacuum, there is no phase shift.

If there is a transparent solid, e.g. glass, in the light path of the interferometer, there is also no phase shift [8]. There is indeed a phase shift by the material, described by the refractive index, but this does not change and overall the symmetry is not broken.

According to Lorentz [9], the refractive index of a material is a consequence of the superposition of the electromagnetic oscillations of the light and the oscillations of the molecules or rather their electric fields.

[1] All data and programmes produced in the course of this research have been published on https://github.com/aetherise/aetherise.

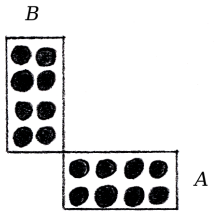

Figure 1: A Michelson interferometer at rest

When one observes light, one always observes the effect of the wave and not the field. The field always propagates at the speed of light, even in the material. But the wave becomes phase-shifted by superposition with other waves. The result is slowed down light.

In Figure 1 a Michelson interferometer is shown. The two arms are marked A and B. The black circles represent the atoms or molecules of matter in the light path. The arms of the interferometer are also made of matter, but are shown simplified as rectangles. The interferometer rests in the aether, so there is no Lorentz contraction. The two arms are approximately the same length and remain so during a rotation.

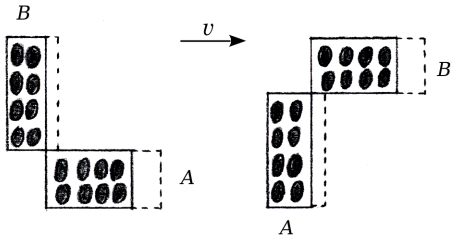

Figure 2: A moving Michelson interferometer

In Figure 2 a moving Michelson interferometer is shown. Once on the left in the initial orientation and once on the right rotated clockwise by 90°. The arrow v indicates the direction of the motion in the aether. One can see the Lorentz contraction of the two arms and of a solid in the path of light. The dashed lines indicate the dimensions of the arms at rest.

As you can see, the number of particles in the light path of both arms remains the same. Therefore there is no change in the phase shift when the orientation is changed.

2.2. Light path in gases

In the gaseous state of aggregation, the individual atoms or molecules of matter can move freely through each other. Each individual particle is contracted in the direction of movement in the aether. However,

the question now arises as to whether the Lorentz contraction also affects the distances between the particles. So whether the density changes like in a solid body.

If you imagine particles that move chaotically and collide with each other, it is not immediately clear what a small change in dimensions will do. Especially when it comes to diatomic molecules, whose shape is very different from that of the sphere.[2]

The hypothesis now is that the density of a gas cloud moving in the aether does not change, at least approximately.

If one operates a Michelson interferometer as an open system in a gas, the result is, according to my hypothesis, a picture as in Figure 3.

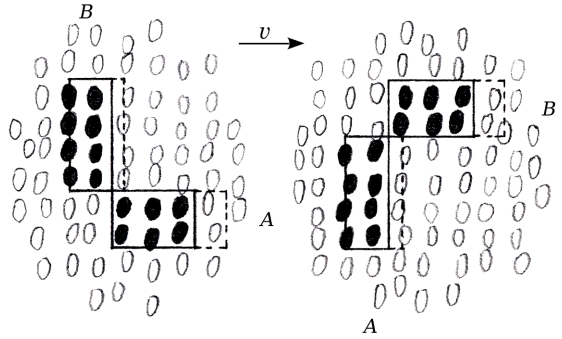

Figure 3: A Michelson interferometer in a gas cloud

In Figure 3, a moving Michelson interferometer is shown inside a co-moving gas cloud. The black ellipses represent the gas molecules that are in the light path of the arms. All the white ellipses are molecules that are outside the light path. Everything else is to be understood as in Figure 2.

It can be seen that in the two different orientations, the number of particles in the light path of the two arms differs. It follows that the phase shift must change with rotation. The symmetry is broken. The phase is no longer Lorentz-invariant and the refractive index becomes anisotropic. A distinction between aether and spacetime is thus possible.

3. Theory

In order to calculate the observed interference fringe shift during a rotation of the interferometer it seems reasonable to develop the theory for a single line segment. You can then calculate any light paths that are composed of individual line segments.

Let S be a coordinate system moving in the aether, and $\vec{v}$ and $\vec{p}$ vectors in this system. The vector $\vec{v}$ indicates the speed and direction of the motion. The vector $\vec{p}$ is the line segment along which a photon moves.

[2] A derivation I will not attempt here.

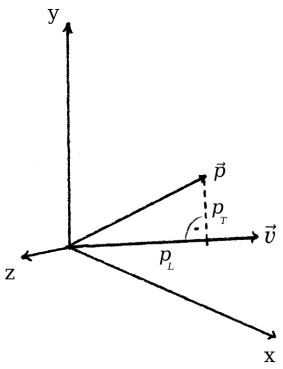

Figure 4: The coordinate system S

3.1. Phase delay

To calculate the time it takes a photon to travel the line segment $\vec{p}$, we determine the longitudinal and transverse part of $\vec{p}$ in the direction of $\vec{v}$. The longitudinal part is

$$p_L = \frac{\vec{v} \cdot \vec{p}}{|\,\vec{v}\,|} \tag{1}$$

und the transverse part is $p_T = |\,\vec{p}_T\,|$, at which

$$\vec{p}_T = \vec{p} - p_L \frac{\vec{v}}{|\,\vec{v}\,|}\ . \tag{2}$$

If u is the velocity of the photon in S, then

$$u_L = \frac{p_L}{|\,\vec{p}\,|} u \quad \text{and} \quad u_T = \frac{p_T}{|\,\vec{p}\,|} u \tag{3}$$

are the longitudinal and transverse components in the direction $\vec{v}$.

With the velocity-addition formula [4] we now transform u from the reference frame S into the reference frame S', the aether:

$$u'_L = \frac{u_L + v}{1 + \frac{u_L v}{c^2}}\ , \quad u'_T = \frac{u_T \sqrt{1 - \left(\frac{v}{c}\right)^2}}{1 + \frac{u_L v}{c^2}}\ . \tag{4}$$

To calculate the time the photon takes to travel $\vec{p}$ in S', we classically determine with the Galilean transformation the speed

$$u'^2 = (u'_L - v)^2 + u'^2_T \tag{5}$$

and, taking into account the Lorentz contraction, the path

$$s'^2 = \left(p_L \sqrt{1 - \left(\frac{v}{c}\right)^2}\right)^2 + p_T^2\ . \tag{6}$$

The time required is then

$$t' = \frac{s'}{u'} \ . \tag{7}$$

We will only calculate times for closed light paths. This means there is no need to ask questions about the correctness and meaning of t' for open paths.

3.2. Phase shift

If one determines the times t_1 and t_2 for two different light paths and forms the difference

$$\Delta t = t_2 - t_1 \ , \tag{8}$$

one can also express this in wavelengths λ

$$\frac{c}{\lambda}\Delta t \ . \tag{9}$$

I assume that the frequency of light in a material always remains the same, even in the gaseous state with Lorentz contraction.

If one determines the Δt for two orientations[3] A and B of the light paths, then

$$\Delta\lambda = \frac{c}{\lambda}(\Delta t_B - \Delta t_A) \tag{10}$$

is the relative displacement in wavelengths.

This calculation yields $\Delta\lambda = 0$ for light paths in vacuum and in solids. For light paths in gases, one must specify a different speed of light for the longitudinal component, due to the changed refractive index n_L. Thus (3) then becomes

$$u_L = \frac{p_L}{|\,\vec{p}\,|}\frac{c}{n_L} \quad \text{and} \quad u_T = \frac{p_T}{|\,\vec{p}\,|}\frac{c}{n} \ . \tag{11}$$

3.3. Anisotropic refractive index

We now want to determine the refractive index n_L of a moving gas in the direction of motion.

In an investigation of the connection between the refractive index n and the body density d, Lorentz [9] finds the quantity

$$\frac{n^2-1}{(n^2+2)d} = R = \text{const.} \tag{12}$$

From a known refractive index n one can now calculate Rd.[4]

Because matter contracts in the direction of motion, and so do all measuring sticks and observers, it looks like in S the density of a gas is lower longitudinally. And exactly by the factor of the Lorentz contraction

$$\frac{1}{\gamma} = \sqrt{1-\left(\frac{v}{c}\right)^2} \ . \tag{13}$$

A different refractive index n_L follows from the changed density. Substituting in (12) and rearranging yields

$$n_L = \sqrt{\frac{1+2Rd\gamma^{-1}}{1-Rd\gamma^{-1}}} \ . \tag{14}$$

So now we have the speed of light we need in (11).

4. Experiment

To test the hypothesis, it was not necessary to conduct an experiment. There have been experiments in the past.

Someone who carried out many experiments and measurements was Dayton C. Miller. In one of his last papers [10] he summarised his results. He came to the conclusion that his data contained a signal from the aether. Miller's work was also criticised [11] and other similar experiments [12] found no signal.

Miller's experiments on Mount Wilson in 1925–1926 were just such experiments, that could test the hypothesis. Mount Wilson is a mountain in California in the United States of America. Miller had carried out extensive systematic measurements there, in four so-called epochs [13]. At the summit at an altitude of 1700 m, a Michelson interferometer was set up in a hut. It was operated as a semi-open system in the air.[5]

The two arms were arranged in a cross shape and consisted of steel girders. The middle part of the steel cross rested on a float. This floated in an annular trough filled with mercury. The whole device weighed 1200 kg. The two steel girders were over 4 m long. At each end there were four mirrors with which the light beams were mirrored several times so that a light path of 64 m was achieved. The light source was an acetylene lamp with a wavelength of 570 nm.

In Figure 5 the hut is shown in which the interferometer is set up. The interferometer is in the orientation at which the measuring process is started. The circle with the 16 graduation marks indicate the azimuths at which a value is read. N, S, W: The cardinal directions. X: The door.[6] T: The four

[3] The relative orientation of the light paths to each other should not change.

[4] Now one can object that all known n are possibly inaccurate because they were determined without taking into account the aether theory. But the accuracy of the absolute value is not decisive because an interferometer measures differences. With the parameter values of the CMB dipole (24), the refractive index 1.00023 would change by 1.7×10^{-10}, resulting in a change in signal amplitude of 1.4×10^{-8} λ.

[5] I call the system semi-open, because the light path was enclosed, but the sides were made of glass. I do not know how tight the cover was.

[6] The hut had, at the level of the arms of the interferometer, continuous rows of windows on each side. These are not drawn in order to increase clarity.

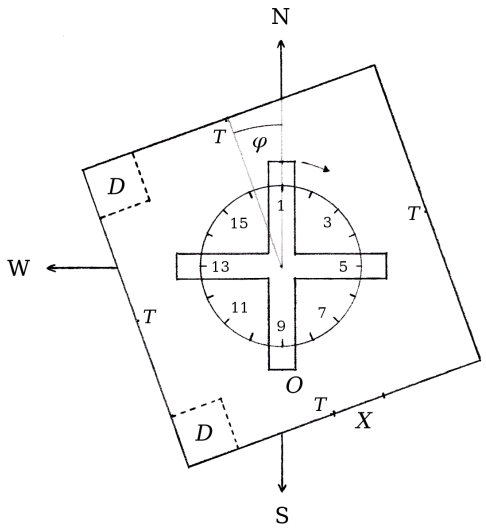

Figure 5: Ground plan of the hut with interferometer

thermometers. D: The two locations of the desk.[7] O: The observer looking through the telescope. φ: Angle of 20° between the perpendicular to the north wall and north. The figure is approximately to scale.

Over the course of a year, Miller carried out four series of observations, each lasting up to two weeks. This resulted in a number of data sheets.

Table 1: Epochs

Epoch	Period	Number
Apr	27.03.1925 – 10.04.1925	36
Aug	24.07.1925 – 08.08.1925	96
Sep	10.09.1925 – 23.09.1925	83
Feb	03.02.1926 – 12.02.1926	101

Each data sheet is usually produced within $\sim$ 15 minutes from 20 turns of the interferometer. At each turn, at the 16 azimuths, the distance of a reference fringe from a mark is read. The value is given in $^1/_{10}$ of a fringe. A data sheet thus consists of a table with the readings and metadata such as time, temperatures and weather conditions.

4.1. Measurement procedure

There is a desk in the hut. Either in the NW corner or in the SW corner, the exact location is not known. At this desk sits the assistant who fills in the data sheet. Miller was not alone in the hut, but had an assistant, R. M. Langer. The interferometer is in a clockwise rotation. After a certain waiting time, the four thermometers are read off and the measurement is started. The interferometer is oriented as in Figure 5, the observer is in the south and looks through the telescope towards the north. Through the telescope the observer sees a number of interference fringes and a mark in the foreground. The observed distance of the reference fringe from the mark is the value for the azimuth 1. The observer moves with the interferometer and for each azimuth tells the observed distance, which is then written down by the assistant.

Unfortunately, the fringe system is at rest only in the very fewest cases. The fringes 'run away', there is a drift in one direction, even if the interferometer has not been set in rotation. The cause in most cases is probably a change in temperature. This causes the the fringe system to move out of the field of view at some point and the interferometer has to be readjusted, so that the reference fringe is again visible near the mark. This adjustment is done with the help of weights that are placed on an arm or removed. If this is not enough, a mirror is readjusted. Presumably with both procedures it can happen that the direction of the fringe displacement changes.

Miller has determined that a certain direction of displacement, which results from a extension of the light path of the arm with the telescope is considered positive. Miller had a possibility to determine this direction, because on many data sheets there is the remark 'Sign correct'.

At the end of the measurement, the thermometers are read again.

[7] I do not know where exactly the desk was positioned, how big it was, and where the assistant sat.

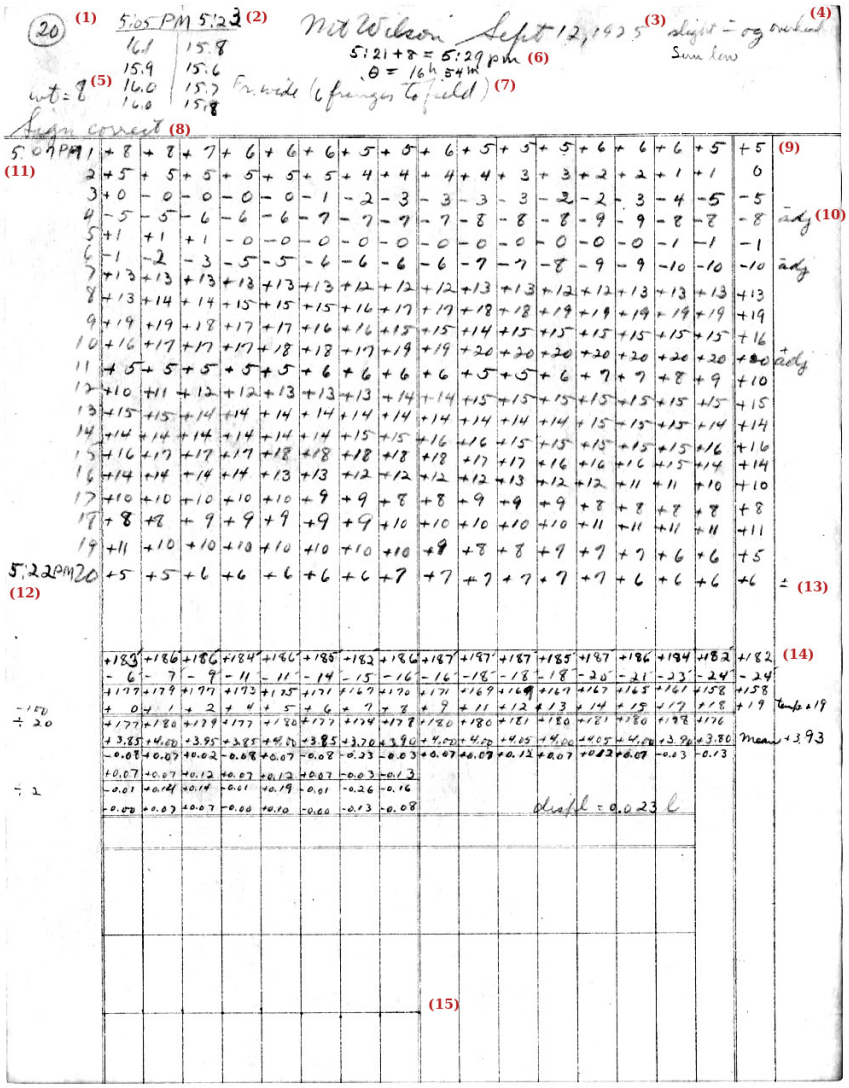

Figure 6: Digital copy of the Sep-20 data sheet from [13].

(1) Consecutively assigned number per epoch.
(2) Table with the temperatures (in °C) of the four thermometers and in the head the reading time. From top to bottom: N, E, S, W.
(3) Title with date.
(4) Weather.
(5) Weight. Probably a number.
(6) Mean observation time + 8 minutes = mean local time. Theta = local sidereal time.
(7) Description of the fringe system.
(8) 'Sign correct': Lengthening the arm with the telescope leads to increasing positive readings.
(9) Table with 20 rows and 16+1 columns. The distances of the reference fringe to the marking in $^1/_{10}$ fringes.
(10) 'adj': Abbreviation for 'adjust'. Adjustment note with sign.
(11) Start of measurement.
(12) End of measurement.
(13) Sign. Here the sign ±.
(14) Data reduction.
(15) Reduced data in a diagram. Only points without connecting lines.

4.2. Data sheets

An example of a data sheet is given in Figure 6. Not all entries are comprehensible. What the number in the weight entry (5) means is not clear. These entries are not consistently maintained and are not taken into account in the data analysis. It is also not clear what the different signs $+, -, \pm, \mp$ at (10) and (13) mean.

The data sheets are used as they are, unclear signs are ignored. Apparently Miller has corrected all data sheets accordingly. A comment on the sign can be found, for example, in data sheet Sep-8. A correction using the sign can be found, for example, in data sheet Sep-9.

The data sheets are available in digitised form, but are not machine-readable. All data sheets were transcribed by hand and a CSV file was created from each individual data sheet.[8] The format of the file is based on the original data sheets.[9]

A few things were changed in the transcription:

1. If on a data sheet only for the beginning or the end of the measurements the temperatures were recorded, then the temperatures were taken from the previous or following data sheet of a group.

2. On the Sep-81 data sheet, the temperature of the west wall thermometer was changed from 13.0 to 13.9. The entry is probably incorrect.

3. On the Sep-50 data sheet, the reading time of the initial temperatures was corrected to 7:58.

4. If column 17 was not filled on a data sheet, then

[8] The files are located in the directory `dcm/csv/`. The digitised originals are not published due to copyright reasons.
[9] A description of the format can be found in the manual of the *aetherise* tool at `aetherise/aetherise_manual.en.pdf`.

for each row the value of column 1 of the following row was entered. For example, for data sheet Sep-1.

5. On some data sheets, some values in column 17 were wrong. It seems that the assistant sometimes took a value from the wrong row. If there is no adjustment note, the value of column 1 of the next line is expected in column 17. If this was not the case, the value was corrected accordingly. Concerns the data sheets Apr-104, Apr-127, Aug-28, Aug-57, Aug-59, Aug-81, Aug-94, Sep-48, Feb-13, Feb-19, Feb-21, Feb-47, Feb-59.

6. If, in a data sheet, the value of column 17 clearly did not match the value of column 1 of the next row and there was no indication of an incorrect value, then the character `a` was added if it was missing. Presumably the adjustment note was forgotten. Concerns data sheets Apr-113, Apr-123, Aug-3, Aug-35, Sep-5, Sep-20, Feb-100.

7. In data sheet Aug-66, the adjustment note at the end has been removed. An adjustment at the end makes no sense.

8. If visitors were present, the names were not transcribed, but only the code `v`. Deciphering the handwriting was too difficult and the names were not considered important.

9. If some of the data sheets have been edited and calculated in different ways, then the calculation or data sheet with a tick was used. A cross is interpreted as *discarded*. The codes `c` and `r` in the last column of the CSV file refer to the selected calculation.

10. If the mean observation time on a data sheet was incorrect, it and all other dependent times were corrected. Concerns data sheets Apr-108, Apr-123, Aug-48, Aug-61, Feb-56, Feb-71. For data sheet Aug-96, the end of observation was calculated from the start time and the mean observation time.

11. If there were further remarks next to or below the table, they were only transcribed if they fit into the subject of the usual remarks in the header of the data sheet, or if they seemed important. Some remarks on the problem of the sign can be found in the transcript of the experiment log.[10]

[10] Located at `dcm/Millers_notes.txt`.

5. Signal

With the theory, one can now calculate the expected signal for Miller's experiment. The signal *Æ* is the displacement of the interference fringes per azimuth during a full rotation of the interferometer. For this one needs the characteristic values for Miller's interferometer, the refractive index of the air, the location on the Earth's surface, the time of the measurement, and the velocity vector of the movement in the aether.

5.1. Known parameters

The characteristic values of the interferometer are known. I calculate simplified with a Michelson interferometer with an arm length of 32.03 m. The geographical coordinates of Mount Wilson are 34.225°N 118.057°W.[11] The date, time and sidereal time are noted on each data sheet. The refractive index is calculated for each data sheet from the given temperatures and weather [14].

A good average value for the temperature in the measurements on Mount Wilson is 13.5 °C. According to the barometric formula, an air pressure of 83 kPa is obtained for a ground temperature of 25 °C at an altitude of 1700 m. With an air pressure of 83 kPa, a temperature of 13.5 °C, a relative humidity of 50 %, a CO_2 concentration of 305 ppm [15], a vacuum wavelength of 570 nm, the refractive index for air is 1.00023.

5.2. Free parameters

The velocity vector in the aether is not known, but one should be able to determine it with the theory from the from the data by using curve fitting. The speed and direction of the movement of the solar system in the aether can be given by the parameters (v, α, δ). Where v here is the speed and (α, δ) the direction in equatorial coordinates. This motion is assumed to be approximately constant.

5.3. Celestial mechanics

Because the Earth rotates on its own axis, the direction of movement in the aether will change for an observer on the Earth's surface in the course of a day.

Because the Earth revolves around the Sun, depending on the orientation of the ecliptic relative to the direction of motion (α, δ), the speed and also the direction of movement in the aether will change in the course of a year. We will not go further into the special cases that exist. The small change caused by the speed of the Earth's own rotation, will be neglected.

[11] https://en.wikipedia.org/wiki/Mount_Wilson_Observatory

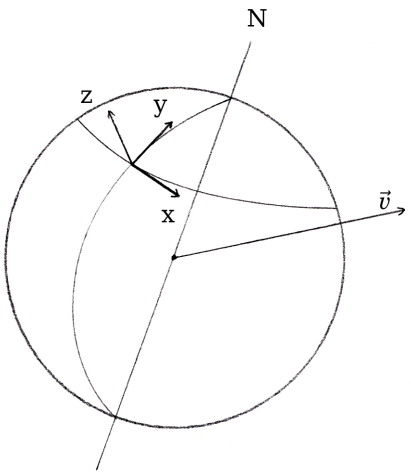

Figure 7: The Earth in the aether with local coordinate system S

We must therefore deal with celestial mechanics, to determine $\vec{v}$ at a given point in time.

In Figure 7 the Earth is shown with its axis of rotation. The north pole is marked N. The origin of the coordinate system S is located at the observation point. The y-axis always points to the north and the z-axis is perpendicular to the surface of the sphere. The velocity vector $\vec{v}$ of the motion in the aether is chosen arbitrarily here.

Earth's rotation

Because S rotates with the Earth, $\vec{v}$ changes in S and this depends on the sidereal time. If the motion of the solar system in the aether is given by the parameters (v, α, δ), we can use the known astronomical coordinate systems to determine the corresponding vector $\vec{v}_S$.[12]

With the sidereal time θ we convert the right ascension α into the hour angle

$$\tau = \theta - \alpha \ . \tag{15}$$

Using the latitude $b = 34.225°$ of the location we determine the horizontal coordinates (a, h)

$$\begin{aligned} \tan(a) &= \frac{\sin(\tau)\cos(\delta)}{\sin(b)\cos(\tau)\cos(\delta) - \cos(b)\sin(\delta)} \\ \sin(h) &= \sin(b)\sin(\delta) + \cos(b)\cos(\delta)\cos(\tau) \ . \end{aligned} \tag{16}$$

Where the azimuth a is measured from the south point, turning positive to the west. If one wants an azimuth measured from the north point, turning positive to the west, one converts a to

$$a_N = -(a + 180°) \ . \tag{17}$$

[12] https://de.wikipedia.org/wiki/Astronomische_Koordinatensysteme

Now we initially place the vector $\vec{v}_S$ so that it points north along the positive y-axis

$$\vec{v}_S = (0, v, 0)^T \ , \tag{18}$$

then we rotate $\vec{v}_S$ around the x-axis by the elevation angle h and then around the z-axis by the azimuth a_N. The vector $\vec{v}_S$ now indicates in S the direction of the movement in the aether.

Earth's orbit

The Earth's orbit is of special importance. Without the Earth's orbit, the movement in the aether would be approximately constant at a given sidereal time, even over the course of a year. This, in conjunction with the symmetry of a Michelson interferometer, means that the direction of the movement cannot be determined unambiguously, because the opposite direction gives the same result. It then holds

$$Æ(\alpha, \delta) = Æ(\alpha + 12 \text{ h}, -\delta) \ . \tag{19}$$

If you take into account the movement of the Earth around the Sun, the signal will change a little, depending on the time of year. The biggest difference is between two signals that are half a year apart. Then the two velocity vectors of the corresponding signals are parallel, but point in different directions. If you have data that are a good half of a year apart, the deviation between theory and data should become smaller, and an unambiguous solution should be found.

In Figure 8 the sun $S_\odot$ and the Earth $E_♁$ are shown. One looks at the north pole of the Earth, which is moving approximately in a circular orbit of radius r in the plane of the ecliptic. The speed and direction of motion at a point in time is given by the vector $\vec{v}_E$. The figure is not to scale.

Since $\vec{v}_E$ is always parallel to a tangent of the orbit at the point of the Earth, one can calculate $\vec{v}_E$ by

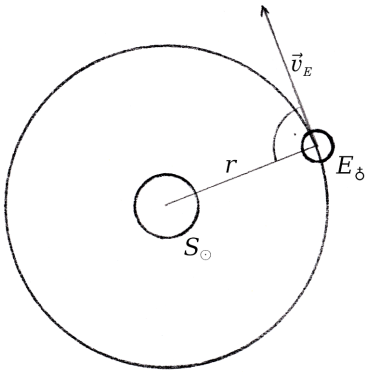

Figure 8: The Earth in its orbit around the Sun

finding the position of the sun, and then shifting that apex in the geocentric ecliptical coordinate system by 90°.

To find the ecliptic coordinates (l, b) of the Sun at the time JD (Julian date) approximation formulas are known:[13]

$$\begin{aligned} m &= JD - 2451545 \\ L &= 280.460^\circ + 0.9856474^\circ \cdot m \\ g &= 357.528^\circ + 0.9856003^\circ \cdot m \\ l &= L + 1.915^\circ \cdot \sin(g) + 0.01997^\circ \cdot \sin(2g) \end{aligned} \tag{20}$$

The ecliptic latitude b is approximately always 0. The apex of the Earth is then

$$(l - 90^\circ, b) \ . \tag{21}$$

After conversion to the equatorial coordinate system with an obliquity of the ecliptic in 1925 of $\epsilon = 23.45^\circ$

$$\begin{aligned} \tan(\alpha) &= \frac{\cos(\epsilon)\sin(l)\cos(b) - \sin(\epsilon)\sin(b)}{\cos(l)\cos(b)} \\ \sin(\delta) &= \cos(\epsilon)\sin(b) + \sin(\epsilon)\cos(b)\sin(l) \ , \end{aligned} \tag{22}$$

and further conversion as from (15), we can finally use the average orbital speed $v_E = 29780$ m/s to form the vector $\vec{v}_E$.

With this one has

$$\vec{v} = \vec{v}_S + \vec{v}_E \ . \tag{23}$$

The theory (10) requires the two vectors $\vec{v}$ and $\vec{p}$ and the refractive index n as parameters. For the period of one or more measurements, $\vec{v}$ and n are approximately constant and only $\vec{p}$ rotates in the xy-plane of S. If one models the light paths of Miller's interferometer, then the theoretical signal is obtained from a full rotation.

5.4. Sign

So far, the direction of the interference fringe displacement was disregarded. We choose the sign in the theory (10) in such a way that a positive value results if in the model of Miller's interferometer, the arm with the telescope is lengthend. This procedure corresponds to the method used by Miller to determine the sign.

5.5. CMB dipole

To get an idea of the signal, one can experimentally insert a vector with cosmologically based values. It seems reasonable to choose the dipole in the cosmic background radiation (CMB), converted into a velocity vector [16]. The parameters are:

$$\begin{aligned} v &= (369.0 \pm 0.9) \text{ km/s} \\ \alpha &= (11.195 \pm 0.005) \text{ h} \\ \delta &= (-6.93 \pm 0.06)^\circ \end{aligned} \tag{24}$$

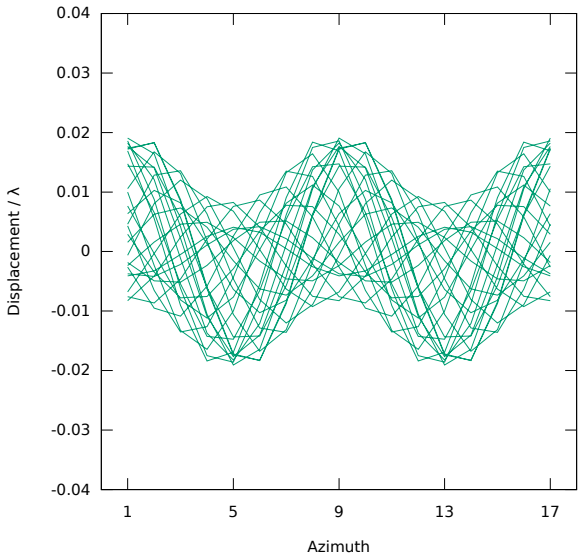

Figure 9: The overlayed theoretical signals of the CMB dipole at different sidereal times [A1]

The signal is a sinusoidal oscillation whose phase and amplitude change with the sidereal time. The signal is periodic in a half-turn. The largest amplitude is ~ 0.02 λ.

In Figure 9 and Figure 10 the theoretical signals calculated with the parameter values of the CMB dipole are shown. The Earth's orbit is not included and the refractive index is fixed at the value 1.00023.

In Figure 11 and Figure 12 one looks along the azimuth axis from Figure 10 and thus sees only the amplitude of the signals. The bumps are caused by the fact that the amplitude is determined from the maximum of the values of the 16 azimuths and the maximum value can also lie between two azimuths. One recognises a slightly asymmetrical dumbbell shape.[14]

In Figure 12, in contrast to Figure 11, the Earth's orbit and the refractive index are included. One can see the influence of the Earth's orbit on the signal, the varying refractive index has hardly any effect. You can see the different signal strengths of the different epochs.

[13] https://de.wikipedia.org/wiki/Sonnenstand

[14] A change in the right ascension α causes a shift of the dumbbell shape in the interval [0, 24) of the sidereal time. An increase in the declination δ causes an increase in the amplitude at 11 h and a decrease of the amplitude at 23 h. A change of the speed v causes a corresponding change in the total amplitude.

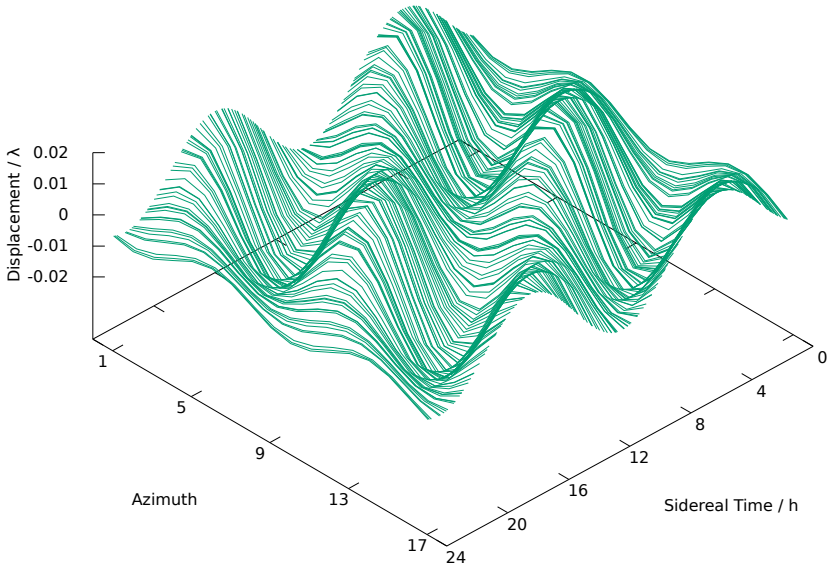

Figure 10: The theoretical signals of the CMB dipole [A2]

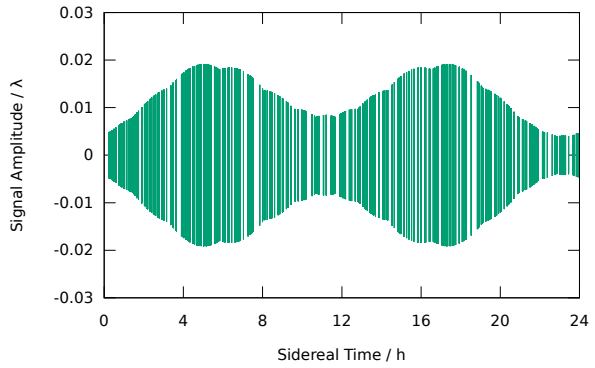

Figure 11: Amplitude of the signals [A3]

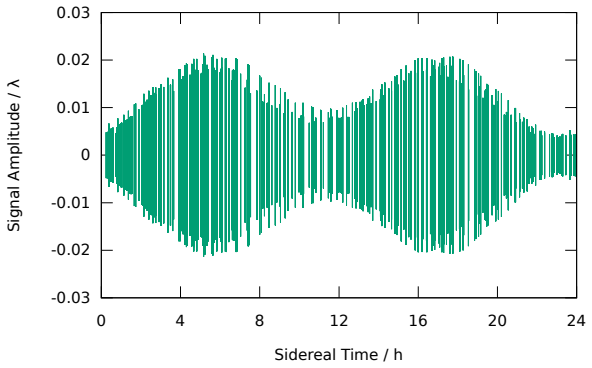

Figure 12: Amplitude of the signals with Earth's orbit and refractive index [A4]

6. Data analysis

In the data analysis, various procedures are presented and applied with which one can find the predicted signal and determine the free parameters. In the analysis the original data with Miller's changes are always used. The tool *aetherise* was developed for data analysis on a computer. All analyses and results presented in this paper can be reproduced in this way.

6.1. Data reduction

The distance æ of a reference fringe to a marker at azimuths i is measured. The distance æ results from the theoretical fringe displacement $Æ$, the offset C of the signal, the drift D, and an unknown systematic error E. The measurement model is

$$\text{æ}_i = Æ_i(\vec{v}, n, i) + C + D_i + E_i \ . \tag{25}$$

The errors C and D can be determined and calculated from the data itself. Let $(q_{ji})_{j=1,\ldots,N;\ i=1,\ldots,17}$ be the table of measured values of a data sheet. After a full rotation j of the interferometer the azimuth 1 is measured twice and the values q_{j1} and q_{j17} are obtained. The drift is then $q_{j17} - q_{j1}$. Assuming that the drift is approximately linear, the drift of the measurement j at the azimuth i is

$$D_{ji} = \frac{q_{j17} - q_{j1}}{16}(i-1) \ . \tag{26}$$

The drift is probably caused by a change in temperature. Other influences that can cause or change a systematic error are shown in Figure 13.

Another systematic error that can be removed is the offset C, which arises through the adjustment and changes due to the drift. Because the initial distance of the reference fringe from the mark at azimuth 1 is arbitrary, all measured values of a turn must be

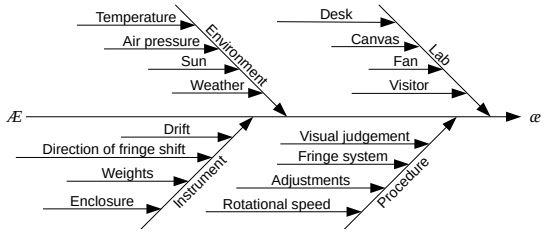

Figure 13: Influences on the measurand

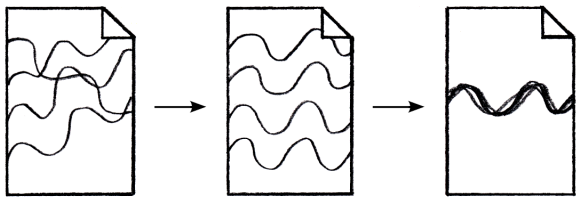

Figure 14: Illustration of the reduction by drift and offset

normalised.

Since one expects a periodic signal and probably also the systematic errors are periodic due to the symmetry of the measuring device, one can calculate C by taking the mean value of all measured values of a measurement j:

$$C_j = \frac{1}{16}\sum_{i=1}^{16} q_{ji} \ . \tag{27}$$

One thus achieves

$$æ_i - C - D_i = Æ_i(\vec{v}, n, i) + E_i \ . \tag{28}$$

When you have reduced the measured values by the drift and the offset, then you calculate

$$q_{ji} \leftarrow \frac{1}{2}(q_{ji} + q_{j(i+8)})_{i=1,\ldots,9} \tag{29}$$

the mean value of opposite azimuths. This reduces the uncertainty and removes systematic errors periodic to a full turn.

Now one can calculate the estimated values $\bar{q}_i$ for (28) from the $(q_{1i}\ q_{2i}\ \ldots\ q_{Ni})^T$ and the uncertainties $u_i = u(\bar{q}_i)$ according to ISO/IEC Guide 98-3 (GUM).[15] From each data sheet you get a record $(\bar{q}_i)_{i=1,\ldots,9}$. This is assigned to the mean observation time.[16] However, the estimated values still contain a systematic error E.

6.2. Signal extraction

An unknown systematic error E, periodic in a half-turn, cannot be calculated from a single data sheet. However, if one has different data sheets A and B and assumes that E is constant under same conditions β

$$\begin{aligned}(\bar{q}_i)_A &\approx (Æ_i)_A + (E_i)\mid_\beta \\ (\bar{q}_i)_B &\approx (Æ_i)_B + (E_i)\mid_\beta \ ,\end{aligned} \tag{30}$$

then one can extract a difference signal

$$(\bar{q}_i)_A - (\bar{q}_i)_B \approx (Æ_i)_A - (Æ_i)_B \ . \tag{31}$$

This is possible because $Æ$ changes over time. The data sheets should have a sufficiently large time distance in order to obtain a strong difference signal.

6.3. Fourier analysis

With a Discrete Fourier Transform (DFT) one can examine any data sheet for existing signals. Before that, the errors C_j and D_{ji} are removed from all q_{ji}.

In Figure 15 the mean spectrum of $\frac{3}{4}$ of all data sheets is shown. Of the 316 data sheets, 242 were used. The data sheets not used were measured under poor temperature conditions or are apparently outliers.[17] The signals of such data sheets typically contain an extraordinarily large amplitude, which would distort the spectrum.

Besides the noise, two clear peaks can be seen at frequencies 1 and 2. *Frequency* here means the number of periods per turn. The corresponding values of the amplitudes can be found in Table 2.

Table 2: Mean amplitudes

Frequency	**Amplitude / λ**
1	0.022
2	0.021

The data reduction in 6.1 and Miller's algorithm behave like a frequency filter, which would also isolate a signal with a frequency ~ 2 from a 1/f noise. However, the algorithm can be used because of the significant signal with frequency 2.

DFT is another data reduction method that we will use. With this method, the required harmonic component $z \in \mathbb{C}$ is determined from the measured values of each turn j. According to GUM, the estimated value $\bar{z}$ and the uncertainties of the components $\Re(\bar{z})$ and $\Im(\bar{z})$ are determined from the $\{z_j\}$.

[15] Miller used an equivalent method for data reduction, but this is not suitable for determining the uncertainties, because the mean value of the measurements at the azimuths is calculated first.

[16] Averaging the variable signals results in a small theoretical error. The maximum deviations from the true signal at the mean observation time are for the amplitude $-9 \times 10^{-6}\ \lambda$, for the phase ± 0.004 h, with an uncertainty at the azimuths of $\pm 0.0001\ \lambda$. Assuming the parameter values of the CMB dipole and a measurement duration of 15 min at 20 turns.

[17] The data sheets in directories `dcm/error/`, `dcm/outlier/`, `dcm/unusual/` were not used.

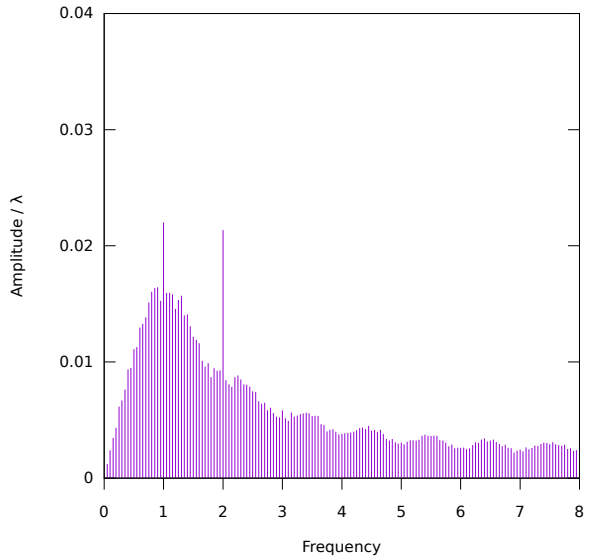

Figure 15: Mean spectrum [A10]

Only the harmonic component with frequency 2 is needed. From each data sheet, one obtains a $\bar{z}$, which corresponds to the $(\bar{q}_i)$ and also to the result of Miller's algorithm, and which can be used in calculations in exactly the same way.

6.4. Normality test

The Shapiro-Wilk test is used to check how well the measured values at the azimuths of the data sheets are are normally distributed.[18] Only in the case of normal distribution can one calculate the standard uncertainties and apply further statistical methods. Before the test, the errors C_j and D_{ji} are removed from all q_{ji}.

The test results follow a binomial distribution with a success probability of $p = 1 - \alpha$ and a rejection rate corresponding to the significance level α if all measurements are normally distributed. If the rejection rate is greater than α, this indicates a genuine proportion of non-normally distributed measurements.

In Table 3 and Table 4, the test results for different categories of data sheets are shown. If you select data sheets according to other criteria such as month, time of day or temperature, similar results are obtained. The average number of measured values per test is 20.

The measurements are normally distributed, with a maximum proportion of $\sim (5 \pm 2)$ % measurements that are not normally distributed.[19] The uncertainty gives an interval for a confidence of 95 %.[20]

6.5. Groups and categories

The data sheets are created in measurement series (groups), usually consisting of 4 or more data sheets. In a group, the epoch and the desk location are the same. If there are more than $\sim$ 1.5 hours between the mean observation time of two consecutive data sheets, a new group is formed. The groups are named according to the epoch and the data sheet number of the first data sheet.

Of the 316 data sheets available, about half are not used. The unused data sheets that were sorted out are grouped into categories according to the reasons given:[21]

canceled Discarded or canceled by Miller.

bad Data sheets whose records have a larger mean uncertainty than $\sim 0.02\ \lambda$.

error Data sheets that probably contain a strong event-related systematic error. For example, if the sun shines on the interferometer. Also a particularly high temperature difference ($\gtrsim 1K$), or a particularly high magnitude temperature change ($\gtrsim 0.5K$) belong to this.

unusual Exceptional data sheets where the normal procedure has been deviated from. For example a different direction of rotation.

outlier Outliers of a group that do not belong to any other category, but nevertheless clearly deviate from the majority.

From the remaining good data sheets, an attempt is made to extract the signals and thus determine the free parameters of the theory.

6.6. Anomalies

Anomalies are groups that can be sorted out less objectively, but are nevertheless conspicuous because they do not confirm an expectation. Anomalies are not found by looking at individual data sheets, but in sequences of data sheets within and between groups.

According to theory, a continuous change of phase and amplitude of the signal is to be expected. Anomalous is, for example, an abrupt strong change in amplitude. To be found in the group Sep-14. In

[18] Function *shapiro.test* in *R* (Version 3.3.3). https://www.r-project.org/

[19] The proportion increases with α and then falls from $\alpha = 0.5$. The reason is unclear. In simple simulations in which a part of randomly generated normally distributed samples were replaced by samples that were clearly not normally distributed, the true proportion remained constant.

[20] The confidence interval is determined using the Agresti-Coull method.

[21] The directory `dcm/csv/` contains correspondingly named subdirectories.

Table 3: Number of azimuths tested [a]

Data Sheets	Rejected at α					Total
	0.5	0.25	0.1	0.05	0.01	
All [A5]	2728	1494	628	330	81	5056
Unused [A6]	1415	779	326	170	42	2656
Usable [A7]	1313	715	302	160	39	2400

[a] The selection of 'Usable' and 'Unused' is described in 6.5.

Table 4: Test rejection rate

Data Sheets	Rate at α / %				
	0.5	0.25	0.1	0.05	0.01
All	54.0 ± 1.4	29.6 ± 1.3	12.4 ± 0.9	6.6 ± 0.7	1.6 ± 0.4
Unused	53.3 ± 1.9	29.4 ± 1.8	12.3 ± 1.3	6.5 ± 1.0	1.7 ± 0.5
Usable	54.7 ± 2.0	29.8 ± 1.9	12.6 ± 1.4	6.7 ± 1.0	1.7 ± 0.5

the groups Aug-31 and Aug-49 there are strong fluctuations of phase and amplitude, which is apparently related to the temperature conditions.

If the same periods have been measured several times under similar conditions, one expects a good agreement of the groups. Anomalous is a clear deviation of phase or amplitude. For example, the Sep-75 group differs from Sep-35 and Sep-8.

6.7. Usability of the groups

In April, groups 107, 110, 113, 117, 122, 130 are usable. Measurements were mainly carried out in two periods of time, 12 h apart. Early in the morning and late evening. In half of the data sheets, the second temperature reading is missing. However, it is possible to estimate the temperature change for successive data sheets.

The entire month of July is dropped. The data sheets all have too much uncertainty or probably a systematic error due to large temperature changes. Miller used apparently a fan, but it was not until August that a tent was erected over the hut.

In August, the groups 29, 60, 74, 80, 86, 88, 91 are usable, but often contain changes of the temperature change. Groups 31 and 49 are anomalies.

In September, groups 1, 22, 26, 35, 49, 57, 63, (75) are usable. Group 14 is an anomaly. Group 75 also stands out because of its high amplitude, but there is no reason not to look for a signal within the group.

In February, groups 18, 21, 43, 47, 53, 69, 74, 77, (80), 92 are usable. Group 95 is discarded due to weather conditions, storm and rain. Group 80 was measured in wind and gusts, so the usability is uncertain.

6.8. Selection of the data sheets

With a few exceptions, Miller's measurements do not match the signals of the CMB dipole.[22] Therefore, I assume that a systematic error periodic in a half-turn is present in almost all measurements. So we will extract differential signals to get rid of the systematic error.

The aim when selecting data sheets for signal extraction is to keep the systematic residual error small. In addition, the difference signal should have an amplitude as large as possible in order to emerge from the noise.

In order to keep the systematic residual error small, only data sheets that were created under similar conditions are selected. The conditions include first of all the epoch and the location of the desk. Further conditions are the temperature difference (TD) in the hut and the mean temperature change (dT). The mean temperature is considered by the theory via the refractive index. One way to specify the TD is to calculate the 'cross difference'

$$T_X = (T_N + T_S) - (T_W + T_E) \; . \qquad (32)$$

T_N here means the temperature of the thermometer of the north wall. The other letters correspond to the respective cardinal directions.

If one assumes that the temperatures have an approximately linear effect, one arrives, by means of symmetry considerations, at the quantity T_X as a measure of the similarity of the TD.[23]

In addition, data sheets from measurements during the day and at night should not be aggregated. Measurements taken at sunrise or sunset are also prob-

[22] The exceptions are the groups Feb-18, Feb-43 and Feb-47.

[23] With other quantities, one finds similar difference signals. For example, you can simply compare all thermometers directly, or – very simplified – use the strongest gradient.

lematic, as the sun is low and can shine into the hut, which Miller also repeatedly notes.

The duration of a turn also seems to have an influence, as can be seen from the data sheets Feb-15 and Feb-16 and on the Sep-57 group. Basically, the duration of a turn is quite constant and only in individual cases attention seems to be necessary.[24]

A large amplitude is achieved when there is sufficient time between the data sheets from which a signal is to be extracted. Here I choose ~ 2 h if possible. For data sheets with low ($< 0.01\ \lambda$) uncertainty, less is also possible.

I choose these values so that the signal-to-noise ratio

$$\frac{\Delta\hat{Æ}}{\bar{u}}\ , \tag{33}$$

the ratio of amplitude of the theoretical difference signal and mean uncertainty of all good data sheets, using the parameter values of the CMB dipole, is at least ~ 1.

If the time interval is too long, this again has a negative effect, because after 12 h the signal can repeat itself, and a difference signal can become weaker again after only 6 h.

6.9. Difference signals

We will extract the difference signals from sequences of data sheets that are as large and similar as possible. We will search within a group and also across groups. The sequences found are first averaged and then the difference signal is calculated.

In order to obtain difference signals that are as good as possible, I set tolerances that determine how big the differences between certain values in the data sheets may be. The adjustable tolerances are the minimum time difference Δt (in h) between two sequences of data sheets, the maximum difference of the temperature difference ΔTD (in °C) and the maximum difference of the mean temperature change ΔdT (in °C per $\frac{1}{4}$h).

A series shall consist of at least two data sheets to ensure similarity of conditions of the measurement series and to reduce the uncertainty. The observed quantities of the data sheets of two series do not have to agree sequentially, but it should be sufficient that a permutation exists in which no tolerances are exceeded.

Two data sheet sequences shall be better than two other data sheet sequences, if they consist of more data sheets or otherwise the sum of the quantities[25]

$$\max\{|\Delta TD_k|\} + \max\{|\Delta dT_k|\} \tag{34}$$

is smaller. For each group and each combination of two groups, the best pair of sequences is used for the signal extraction.

I choose small tolerances first and then increase them until a sufficient sidereal time coverage is achieved by the data sheets. One can start with $\Delta t = 1$ and $\Delta TD = 0.1$ and $\Delta dT = 0.1$. By trial and error I then find the tolerances $\Delta t = 0.9$ and $\Delta TD = 0.3$ and $\Delta dT = 0.25$.

I choose the Δt and ΔTD so that the only signal from April is still found. I further increase the ΔdT from 0.2 to 0.25 because this will improve the result later.[26] A larger outlier would appear, which is prevented by a slightly different data sheet selection. Furthermore, later the goodness of fit in Table 6 would not change as expected.

In Table 5 the selected difference signals have a number and the unused ones have no number. The difference signal is given by an expression for signal extraction, as it is also output by *aetherise*. The expression consists of the epoch and two intervals which indicate a sequence of data sheet numbers. The remarks consist mainly of reasons why some signals were not used.

In Figure 16 the temporal intervals of the used data sheet sequences are translucent so that overlaps can be recognised. Winter consists of the epochs February and April, summer consists of the epochs August and September. In addition, the amplitude of the theoretical signal, calculated with the parameter values of the CMB dipole (24), also separated into winter and summer, is shown. The difference signal 5 is missing here due to the uncertain usability of the group Feb-80.

In the case of the CMB dipole, the two amplitude minima at 11 h and 23 h would be well hit, and the highest amplitudes would also be covered. There would also be enough data sheets in summer as well as in winter, in order to enable the unambiguous determination of the apex of the movement in the aether on the basis of the amplitude.

6.10. Curve fitting

If one has a number N of extracted difference signals $\{(\Delta q_i)_k\}$ or $\{\Delta z_k\}$, one can now try to find the free parameters (v, α, δ). To do this, we use the chi-squared test (χ^2 test) and minimise the quantity χ^2.

We will not calculate directly with the Δq_i, but determine for each Δz the phase $\tilde{z}$ and amplitude $\hat{z}$ and their uncertainties $\tilde{u}$ and $\hat{u}$. A theoretical difference signal $\Delta Æ$ has the phase $\tilde{Æ}$ and the amplitude $\hat{Æ}$.

[24] Changing the selection for the Sep-57 group would hardly change the result later when minimising.

[25] Here, different quantities with different units are added.

[26] This procedure can be seen as a regression step.

Table 5: Found and selected difference signals [A8]

No.	Difference Signal		Remark
	Within groups		
	aug	[31, 33] - [34, 36]	Anomaly Aug-31
1	sep	[49, 51] - [52, 54]	
2	sep	[57, 58] - [60, 61]	
3	sep	[78, 79] - [81, 82]	
4	feb	[48, 49] - [51, 52]	
5	feb	[85, 87] - [89, 91]	Wind and gust
	Between groups		
6	apr	[110, 111] - [113, 114]	
	aug	[29, 30] - [49, 50]	Anomaly Aug-49
	aug	[32, 33] - [52, 53]	Anomaly Aug-31
	aug	[31, 33] - [60, 62]	Anomaly Aug-31
	aug	[49, 51] - [60, 62]	Anomaly Aug-49
	aug	[76, 77] - [86, 87]	Groups overlap and are clearly different.
7	sep	[39, 42] - [53, 56]	
8	feb	[25, 26] - [45, 46]	
9	feb	[25, 26] - [50, 51]	
10	feb	[44, 46] - [50, 52]	
	feb	[50, 51] - [53, 54]	Difference from groups with rising and falling temperatures.
11	feb	[74, 75] - [77, 78]	

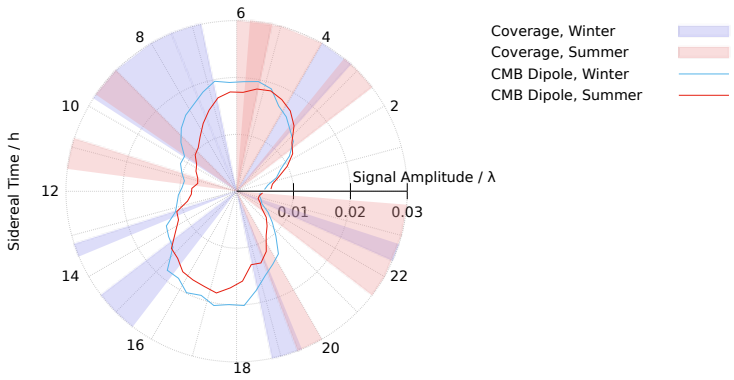

Figure 16: Coverage of the sidereal time by the difference signals [A9]

We then minimise

$$\chi^2 = \sum_{k=1}^{N} \left(\frac{\tilde{z}_k - \tilde{Æ}_k(v,\alpha,\delta)}{\tilde{u}_k} \right)^2 + \sum_{k=1}^{N} \left(\frac{\hat{z}_k - \hat{Æ}_k(v,\alpha,\delta)}{\hat{u}_k} \right)^2 . \quad (35)$$

The uncertainties of the parameters at the minimum are determined with the method $\Delta\chi^2 = 1$.

One should not calculate directly with the Δq_i of all difference signals, because this will probably reduce the amplitude of the theoretical signals. That this is the case can easily be seen by trying to fit a sinusoidal function to two equal, slightly out-of-phase signals.

The number of degrees of freedom is theoretically

$$f = 2N - 3 , \quad (36)$$

because we have 2 values – phase and amplitude – for N difference signals and 3 parameters. Whether one may calculate f in this way is questionable. The rather complicated theory could have non-trivial degrees of freedom [17]. In simulations, the validity of (36) was confirmed.

6.11. Test for signal content

Once the free parameters have been determined, one can check whether a group of data sheets contains the time-varying theoretical signal. Again, it is assumed that the systematic error is constant.

If one subtracts the theoretical signal from a group, then the constant systematic error should remain. The records thus become more similar. If the theory is added to a group, then the similarity should decrease.

To determine the similarity of records, we use a similar sum to that used for the quantity χ^2. The quantity

$$R^2 = \sum_i \left(\frac{\bar{q}'_i - \bar{q}_i}{\sqrt{u_i^2 + u_i'^2}} \right)^2 \quad (37)$$

is a measure of the deviation of two records $(\bar{q}_i)$ and $(\bar{q}'_i)$ with their uncertainties (u_i) and (u'_i). The smaller the quantity, the greater the similarity.

In theory, however, there are also periods in which the signal hardly changes or is very weak, which is why this method then fails.

6.12. Simulations

A simulation is a simulated measurement of a data sheet. All measured data of a data sheet are replaced by calculated values. The calculation is given by (25). The drift D is taken from the measurement data. The E_i are calculated by assuming a systematic error periodic in a half-turn and a systematic error periodic in a turn. The phase and amplitude of both errors are additionally modified by a normally distributed statistical error. The phase of $Æ$ is also shifted a little further with each measurement to create uncertainty. Each simulated measured value finally is modified by a normally distributed statistical error.

The simulation was set up to produce a similar picture in the raw data diagram and similar uncertainties. The templates were the good data sheets. In addition, no systematic residual error should remain when the difference signals are extracted.

The systematic error periodic to a turn and rounding to an accuracy of $^1/_{10}$ of a fringe provide for a proportion of non-normally distributed simulated measurement data. The proportion is with ~ 6 % similarly high as in the real measurement data.

Simulations can be used to test all the methods presented here. The simulations show that basically all methods work. With the difference signals found, the true parameter values can reliably be determined by curve fitting.

7. Results

7.1. Curve fitting

The minimisation was carried out numerically on a computer with the programme *aetherise*. During the minimisation, the difference signal 5 stands out. It is almost a zero line and thus carries hardly any phase information. Due to the known uncertain usability it is switched off in all calculations.

In Table 6, different variants of calculating the theoretical signal and the results of the curve fitting are given. One variant is to neglect the velocity vector of the Earth in its orbit around the Sun. Another variant is to set the refractive index n to a fixed mean value instead of calculating it from temperature and weather. The uncertainties are 1-sigma standard uncertainties without consideration of covariances and without specification of the systematic error.

The parameters of the first line in Table 6 are the main result of this work:

$$\begin{aligned} v &= (326 \pm 17) \text{ km/s} \\ \alpha &= (11.0 \pm 0.2) \text{ h} \\ \delta &= (-11 \pm 5)^\circ \end{aligned} \quad (38)$$

The associated χ^2 statistic is rather poor, indicating that there are deviations that are unlikely to be due to chance.

Another statistic is the distribution of the residuals, whose squares sum to χ^2. The histogram of the

Table 6: Parameters at the minimum and statistics [a]

Variant	v / km/s	α / h	δ / deg	χ^2/f	p
With Earth's orbit, n calculated [A11]	326 ± 17	11.0 ± 0.2	-11 ± 5	2.144	0.004
With Earth's orbit, n=1.00023 [A12]	326 ± 17	11.0 ± 0.2	-11 ± 5	2.150	0.004
Without Earth's orbit,[b] n calculated [A13]	336 ± 17	11.1 ± 0.2	-10 ± 5	2.284	0.002
Without Earth's orbit,[b] n=1.00023 [A14]	335 ± 17	11.1 ± 0.2	-10 ± 5	2.292	0.002

[a] The number of degrees of freedom $f = 17$ was confirmed by simulations.
[b] Second minimum at (α, δ) = (23.1, 10). The other parameter values, uncertainties and statistics are the same.

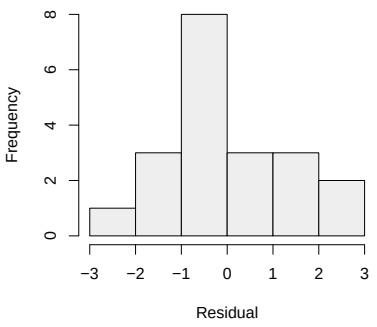

Figure 17: Histogram of the residuals [A15]

residuals is shown in Figure 17. If one assumes a normal distribution, then one expects $\mu = 0$ and $\sigma^2 = 1$ for its parameters. The determined parameter values are $\mu = -0.050$ and $\sigma^2 = 1.9$. A Shapiro-Wilk test for normal distribution yields a p-value of $p = 0.36$.[18]

Except for the σ^2 variance, the statistics are good. The poor χ^2 statistic and the high variance can be explained by a normally distributed systematic residual error in the difference signals.

7.2. Test for signal content

With the parameter values (38) found, one can now test for signal content in groups with constant conditions. The groups from which the difference signals were extracted are used here.

Table 7: Similarity of data sheet sequences

Data Sheets	R^2	R^2_-	R^2_+	Δ
Sep [39, 42] [A17]	16.29	17.34	15.80	-1.54
Sep [49, 56]	11.66	11.45	16.14	4.69
Sep [57, 62]	40.46	38.26	46.25	7.99
Sep [78, 83]	47.81	48.69	50.31	1.62
Feb [48, 52]	7.91	8.75	10.47	1.72
Feb [74, 79]	9.80	9.73	21.57	11.84
Feb [85, 91]	24.02	26.88	23.35	-3.53

Due to the good agreement of the found parameter values (38) with the values of the CMB dipole (24), it is interesting to carry out the test for signal content with these values.

Table 8: Similarity of data sheet sequences when using the parameters of the CMB dipole

Data Sheets	R^2	R^2_-	R^2_+	Δ
Sep [39, 42] [A18]	16.29	18.13	15.37	-2.76
Sep [49, 56]	11.66	12.81	18.93	6.12
Sep [57, 62]	40.46	37.96	48.21	10.25
Sep [78, 83]	47.81	49.40	51.98	2.58
Feb [48, 52]	7.91	9.25	11.74	2.49
Feb [74, 79]	9.80	12.45	29.38	16.93
Feb [85, 91]	24.02	28.10	23.45	-4.65

In Table 7 and Table 8 the mean similarity of successive data sheets is given in the column R^2. In the column R^2_- the theory was previously subtracted, in the column R^2_+ the theory was previously added. In the column Δ the difference $\Delta = R^2_+ - R^2_-$ is given. The data sheets used are given by the epoch and an interval of the data sheet numbers.

It can be seen that R^2_- is often not smaller than R^2 at all, but is still smaller than R^2_+. This behaviour was confirmed in simulations. The deterioration of the similarity by addition of the theory is clearly greater than the improvement by subtraction of the theory. A positive value for Δ can be taken as confirmation.

7.3. Further results

The anisotropy of the mean speed of light on closed paths can be given by the relative change of the refractive index $\Delta n/n = (n - n_L)/n$. The refractive index is set to an average value of $n = 1.00023$. With the CMB dipole (24), the theoretical result is $\Delta n/n = 1.7 \times 10^{-10}$, measured (38) was $\Delta n/n \sim 1.4 \times 10^{-10}$.

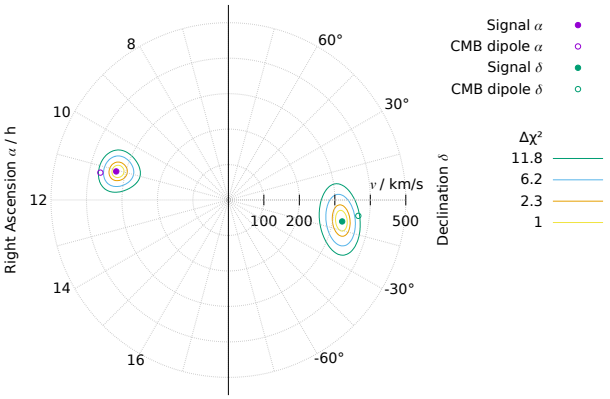

Figure 18: The parameters (v, α, δ) at the minimum.[A16a]

The right ascension and declination have their own scale, the origin is identical. The parameters are shown in pairs as polar coordinates (v, α) and (v, δ) with their $\Delta\chi^2$ isolines. For comparison of the parameter values with those of the CMB dipole, the latter is also shown.

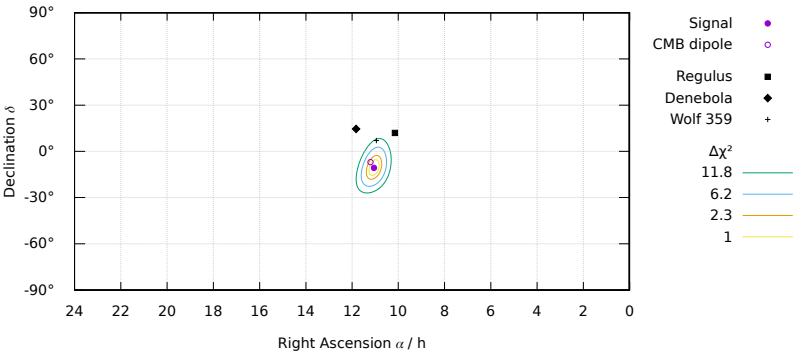

Figure 19: Apex of the motion in the aether.[A16b]

Here the parameter pair (α, δ) is shown at the minimum with its $\Delta\chi^2$ isolines. To compare the parameter values with those of the CMB dipole, the latter is also shown. In addition, some stars of the constellation Leo are shown.

7.4. Difference signals

Here, all extracted difference signals are shown together with the theoretical difference signal in diagrams.[A19] The theory is calculated with the parameter values of the CMB dipole. The title of each diagram corresponds to the expression for signal extraction. The records have been reduced to a single period using Miller's algorithm, but two periods are shown.

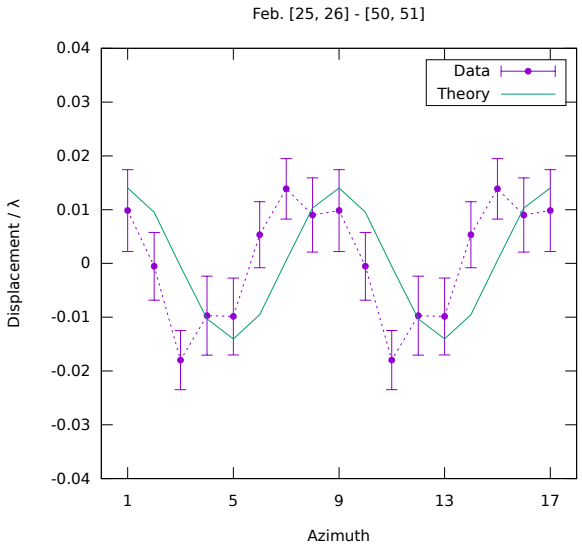

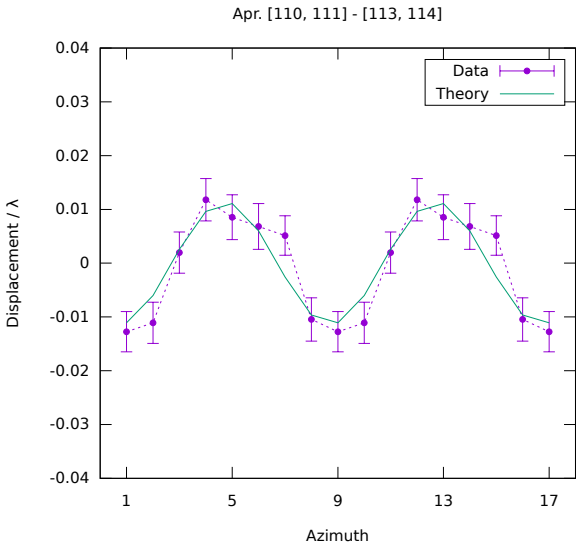

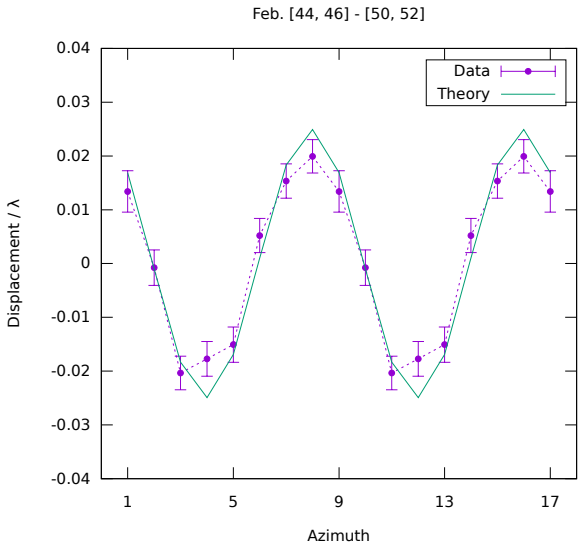

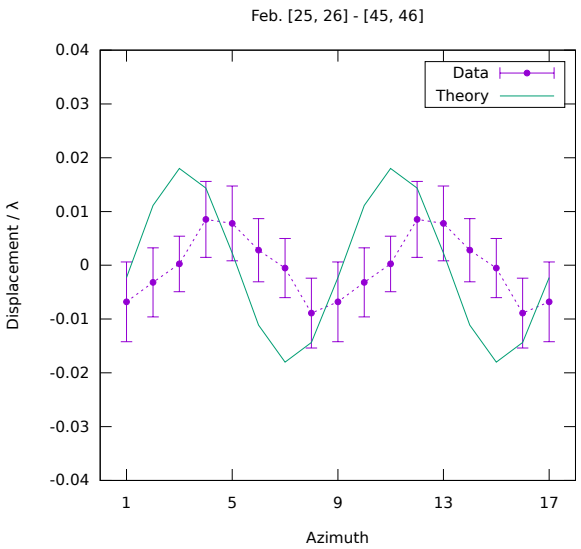

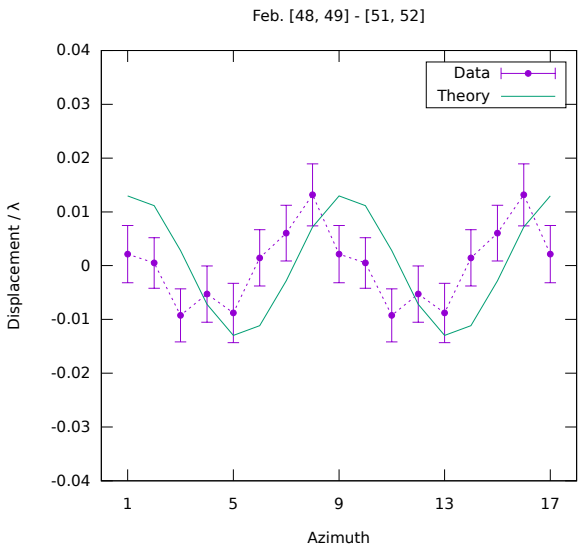

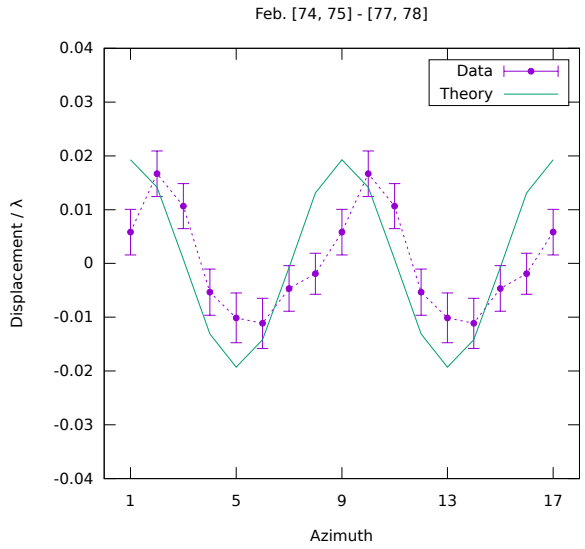
Feb. [74, 75] - [77, 78]
Data
Theory
Displacement / λ
Azimuth
0.04
0.03
0.02
0.01
0
-0.01
-0.02
-0.03
-0.04
1
5
9
13
17

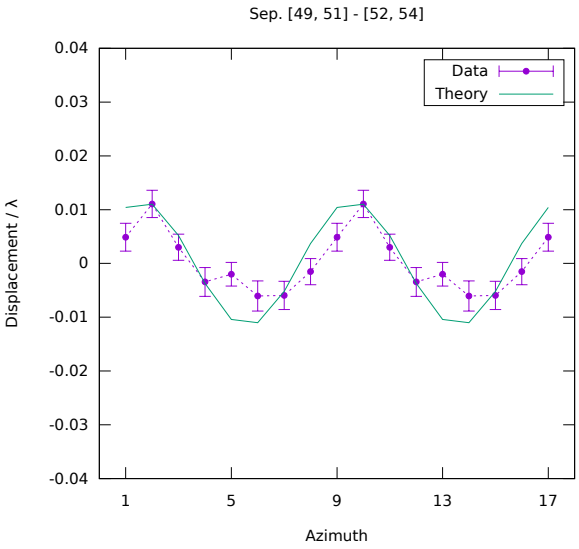
Sep. [49, 51] - [52, 54]
Data
Theory
Displacement / λ
Azimuth
0.04
0.03
0.02
0.01
0
-0.01
-0.02
-0.03
-0.04
1
5
9
13
17

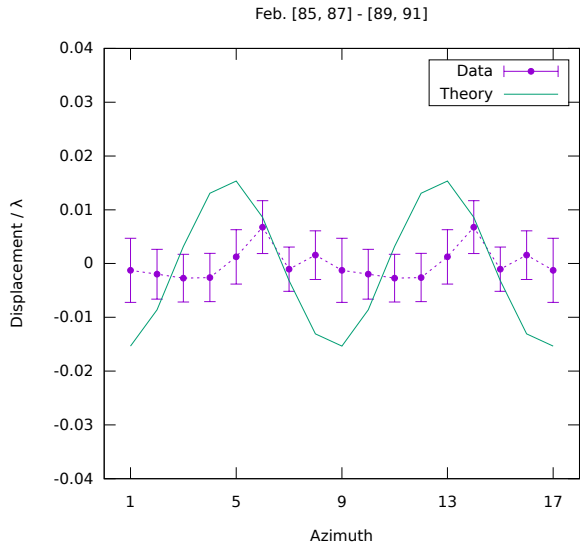
Feb. [85, 87] - [89, 91]
Data
Theory
Displacement / λ
Azimuth
0.04
0.03
0.02
0.01
0
-0.01
-0.02
-0.03
-0.04
1
5
9
13
17

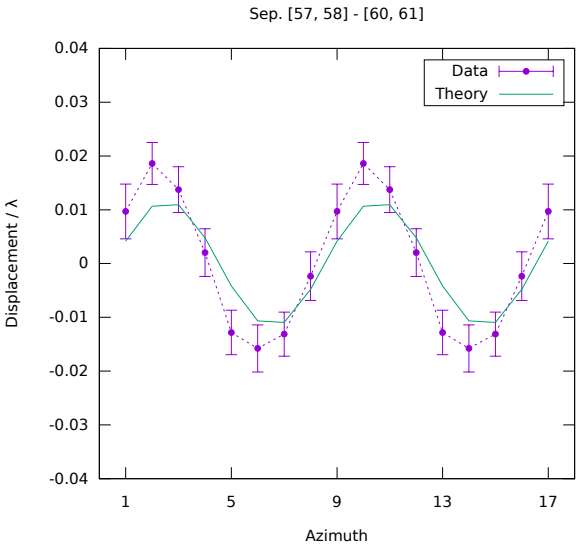
Sep. [57, 58] - [60, 61]
Data
Theory
Displacement / λ
Azimuth
0.04
0.03
0.02
0.01
0
-0.01
-0.02
-0.03
-0.04
1
5
9
13
17

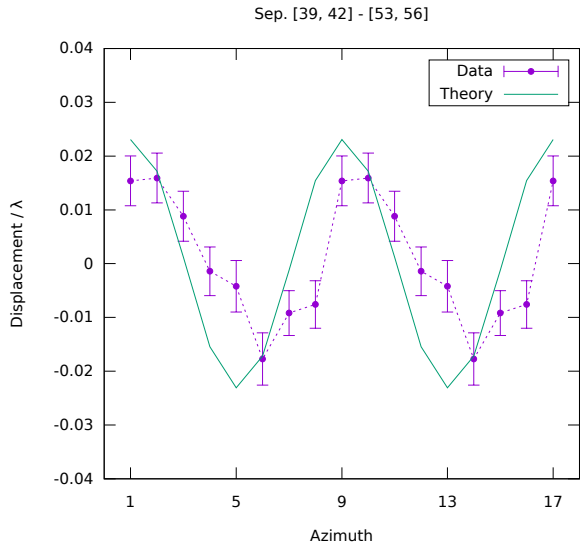
Sep. [39, 42] - [53, 56]
Data
Theory
Displacement / λ
Azimuth
0.04
0.03
0.02
0.01
0
-0.01
-0.02
-0.03
-0.04
1
5
9
13
17

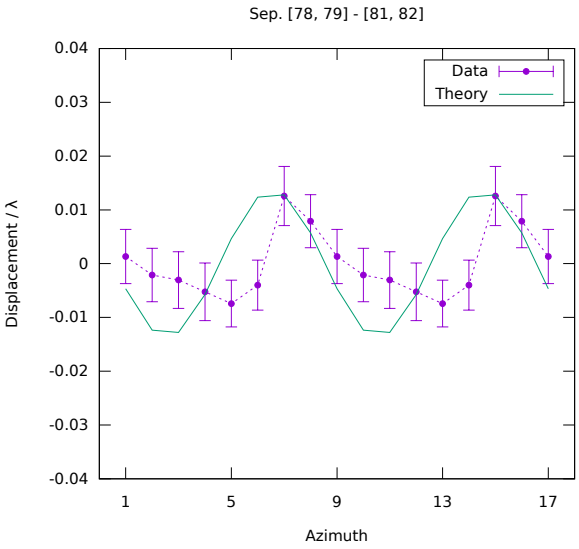
Sep. [78, 79] - [81, 82]
Data
Theory
Displacement / λ
Azimuth
0.04
0.03
0.02
0.01
0
-0.01
-0.02
-0.03
-0.04
1
5
9
13
17

8. Conclusions

Due to the agreement of the parameter values found with the values of the CMB dipole, I assume that this is what was measured. The most obvious interpretation of the CMB dipole as a Doppler effect, due to a movement relative to an isotropic CMB, is thus confirmed. This motion is the absolute motion we are looking for. The reference frame of the aether is thus identical with the the rest frame of the CMB.[27]

The good agreement, despite rather poor statistics, is probably due to the fact that the systematic residual errors are randomly distributed and for the most part cancel each other out.

That there really is a signal in Miller's data is confirmed by the results found. In Table 6 the goodness of fit deteriorates according to the chosen variant. The refractive index has a small effect, the Earth's orbit a larger one. In Table 7 and 8 the similarity changes as required, with small exceptions.

This confirms the aether theory and my hypothesis. And in a way that does not confirm STR, because according to STR there should be no signal. Using the STR one would have to explain how the 3.4 mK of the CMB dipole [16] influence Miller's experiment in such a way that the signal found is measured. Should this not succeed, special relativity, and with it the space-time interpretation of the Lorentz transformation, is disproved.

The initial question as to the true meaning of the Lorentz transformation can only be partially answered because Miller's experiment does not make any statement about the isotropy of the speed of light in a vacuum. However, the following statements are possible: There is an preferred reference frame, the aether. In the aether, the electric and magnetic fields propagate at the speed of light. There is a real physical contraction of the fields at a relative movement of the field sources with respect to the aether.

All bodies of the solar system thus move, Lorentz-contracted, with about $^1/_{1000}$ of the speed of light, through the aether in the direction of the constellation Leo.[28]

To be certain, Miller's experiment must of course be repeated and confirmed. There will probably be other ways to measure violations of Lorentz invariance. Miller [10] has mentioned several other works in which a signal was measured. What is often missing from these and other works is a theoretical explanation by aether theory. It is also not clear why in some repetitions of Miller's experiments no signal was measured. The aether theory will provide new insights into all these questions and ambiguities.

The results of this work are convincing and I think one can justifiably claim:
The aether has been discovered.

[27] The rest frame of the CMB is the reference frame in which the dipole disappears, i.e. the CMB appears isotropic.

[28] Gravity was not considered in this work and it is not clear to me whether the gravitational field, i.e. the orbits of the celestial bodies, are also Lorentz-contracted.

A. Commands

List of commands used to generate data for tables and diagrams. The Aetherise project 1.0.0 was used. The operating system used is a Linux-like one.

A1. `aetherise dcm/csv/*.csv dcm/csv/*/*.csv -reduce -no_data -disable_earth -n 1.00023 -month [9,9] -no [75,77] -no [79,81] -no [83,83] -no [43,43] -no [67,67] -no [69,69] -no [57,57] -no [59,59] -no [60,60] -no [62,62] -no [14,14] -no [16,17] -no [19,20] -no [65,65] -no [29,29] -no [31,33] -no [55,56] > s.dat`

   a) `plot_signal.sh s.dat "" image.svg`

A2. `aetherise dcm/csv/*.csv dcm/csv/*/*.csv -reduce -no_data -disable_earth -n 1.00023 -time [0,12] > s.dat`

   a) `plot_signal3d.sh s.dat "" image.svg`

A3. `aetherise dcm/csv/*.csv dcm/csv/*/*.csv -reduce -no_data -disable_earth -n 1.00023 > s.dat`

   a) `plot_theory_amp.sh s.dat "" image.svg`

A4. `aetherise dcm/csv/*.csv dcm/csv/*/*.csv -reduce -no_data > s.dat`

   a) `plot_theory_amp.sh s.dat "" image.svg`

A5. `test_for_normality.R -ignore_all dcm/csv/*.csv dcm/csv/*/*.csv`

A6. `test_for_normality.R -ignore_all dcm/csv/*/*.csv`

A7. `test_for_normality.R -ignore_all dcm/csv/*.csv`

A8. `aetherise -single -ignore all dcm/csv/*.csv -aggregate signals -signals_dt 0.9 -signals_dTD 0.3 -signals_ddT 0.25`

A9. `aetherise dcm/csv/*.csv dcm/csv/*/*.csv -aggregate sidereal -month [2,4] -no_data > s.dat`

   a) `aetherise dcm/csv/*.csv dcm/csv/*/*.csv -aggregate sidereal -month [7,9] -no_data >> s.dat`

   b) `plot_coverage.sh selected_signals_coverage.dat s.dat "" image.svg`

A10. `aetherise -ignore all dcm/csv/*.csv dcm/csv/bad/*.csv -spectrum -aggregate mean > s.dat`

   a) `plot_spectrum.sh s.dat "" image.svg`

A11. `aetherise -single -ignore all dcm/csv/*.csv -reduction DFT -aggregate fit -fit_sine -fit_disable 5 < selected_signals.txt`

A12. `aetherise -single -ignore all dcm/csv/*.csv -reduction DFT -aggregate fit -fit_sine -fit_disable 5 -n 1.00023 < selected_signals.txt`

A13. `aetherise -single -ignore all dcm/csv/*.csv -reduction DFT -aggregate fit -fit_sine -fit_disable 5 -disable_earth < selected_signals.txt`

A14. `aetherise -single -ignore all dcm/csv/*.csv -reduction DFT -aggregate fit -fit_sine -fit_disable 5 -disable_earth -n 1.00023 < selected_signals.txt`

A15. `aetherise -single -ignore all dcm/csv/*.csv -reduction DFT -aggregate fit -fit_sine -fit_disable 5 -stats -residuals < selected_signals.txt > r.dat`

   a) `histcsv.R r.dat 1 Residual Frequency image.pdf`

A16. `aetherise -single -ignore all dcm/csv/*.csv -reduction DFT -aggregate fit -fit_sine -fit_disable 5 -contour -delta_chi2 16 < selected_signals.txt > c.dat`

a) `plot_contour.sh c.dat "" image.svg`

b) `plot_contour_apex.sh c.dat "" image.svg`

A17. Examples of how the values of the columns R^2, R^2_-, R^2_+ of Table 7 were determined

a) `aetherise -single -ignore all dcm/csv/*.csv -aggregate diff -theory_params 326000,11,-11 -month [9,9] -no [39,42]`

b) `aetherise -single -ignore all dcm/csv/*.csv -aggregate diff -theory_params 326000,11,-11 -month [9,9] -no [39,42] -subtract_theory`

c) `aetherise -single -ignore all dcm/csv/*.csv -aggregate diff -theory_params 326000,11,-11 -month [9,9] -no [39,42] -add_theory`

A18. Examples of how the values of the columns R^2, R^2_-, R^2_+ of Table 8 were determined

a) `aetherise -single -ignore all dcm/csv/*.csv -aggregate diff -month [9,9] -no [39,42]`

b) `aetherise -single -ignore all dcm/csv/*.csv -aggregate diff -month [9,9] -no [39,42] -subtract_theory`

c) `aetherise -single -ignore all dcm/csv/*.csv -aggregate diff -month [9,9] -no [39,42] -add_theory`

A19. Example of signal extraction and generation of the diagrams

a) `aetherise -single -ignore all dcm/csv/*.csv -reduce -aggregate mean -month [3,4] -no [113,114] -csv > data.csv`

b) `aetherise -single -ignore all dcm/csv/*.csv -reduce -aggregate mean -month [3,4] -no [110,111] -data data.csv -subtract_data > s.dat`

c) `plot_signal.sh s.dat "Apr. [110, 111] - [113, 114]" image.svg`

References

[1] Sebastian Pliet. 'Hypothese einer Verletzung der Lorentz-Invarianz in der Äthertheorie und Bestätigung durch die Experimente von D. C. Miller'. 2021. URL: https://vixra.org/abs/2104.0040.

[2] Henri Poincaré. 'Sur la dynamique de l'électron'. In: *Comptes rendus de l'Académie des Sciences de Paris* 140 (1905), pp. 1504–1508.

[3] Hendrik A. Lorentz. 'Elektromagnetische Erscheinungen in einem System, das sich mit beliebiger, die des Lichtes nicht erreichender Geschwindigkeit bewegt'. In: *Das Relativitätsprinzip – Eine Sammlung von Abhandlungen*. B. G. Teubner, 1913, pp. 6–26.

[4] Albert Einstein. 'Zur Elektrodynamik bewegter Körper'. In: *Annalen der Physik und Chemie* 17 (1905), pp. 891–921.

[5] Hermann Minkowski. 'Raum und Zeit'. In: *Physikalische Zeitschrift* 10 (1909), pp. 104–111.

[6] Albert A. Michelson and Edward W. Morley. 'On the Relative Motion of the Earth and the Luminiferous Ether'. In: *American Journal of Science* 34 (1887), pp. 333–345.

[7] Hendrik A. Lorentz. 'Die relative Bewegung der Erde und des Äthers'. In: *Abhandlungen über Theoretische Physik*. B. G. Teubner, 1907, pp. 443–447.

[8] J. Shamir and R. Fox. 'A New Experimental Test of Special Relativity'. In: *Nuovo Cimento B* 62 (1969), p. 258.

[9] Hendrik A. Lorentz. 'Ueber die Beziehung zwischen der Fortpflanzungsgeschwindigkeit des Lichtes und der Körperdichte'. In: *Annalen der Physik und Chemie* IX (1880), pp. 641–665.

[10] Dayton C. Miller. 'The Ether-Drift Experiment and the Determination of the Absolute Motion of the Earth'. In: *Reviews of Modern Physics* 5 (1933), pp. 203–242.

[11] R. S. Shankland et al. 'New Analysis of the Interferometer Observations of Dayton C. Miller'. In: *Reviews of Modern Physics* 27 (1955), pp. 167–178.

[12] Georg Joos. 'Die Jenaer Wiederholung des Michelsonversuchs'. In: *Annalen der Physik* 7 (1930), pp. 385–407.

[13] 19IM2 Dayton C. Miller Papers, 1878-1939, Case Western Reserve University Archives.
19IM2 6:17 Research. Interferometer. Mt. Wilson, April 1925
19IM2 6:18 Research. Interferometer. Mt. Wilson, July-August 1925
19IM2 6:19 Research. Interferometer. Mt. Wilson, July-August 1925
19IM2 7:1 Research. Interferometer. Mt. Wilson, September 1925
19IM2 7:2 Research. Interferometer. Mt. Wilson, September 1925
19IM2 7:3 Research. Interferometer. Mt. Wilson, February 1926
19IM2 7:4 Research. Interferometer. Mt. Wilson, February 1926.

[14] Philip E. Ciddor. 'Refractive index of air: new equations for the visible and near infrared'. In: *APPLIED OPTICS* 35 (1996). URL: https://emtoolbox.nist.gov/Wavelength/Ciddor.asp.

[15] D. M. Etheridge et al. 'Historical CO2 Records from the Law Dome DE08, DE08-2, and DSS Ice Cores (1006 A.D.-1978 A.D)'. In: *Carbon Dioxide Information Analysis Center* (1998). URL: https://cdiac.ess-dive.lbl.gov/ftp/trends/co2/lawdome.smoothed.yr20.

[16] G. Hinshaw et al. 'Five-Year Wilkinson Microwave Anisotropy Probe (WMAP) Observations: Data Processing, Sky Maps, and Basic Results'. In: *Astrophys.J.Suppl* 180 (2009), pp. 225–245. URL: https://arxiv.org/abs/0803.0732v2.

[17] R. Andrae et al. 'Dos and don'ts of reduced chi-squared'. 2010. URL: https://arxiv.org/abs/1012.3754.